Chinese Journal of Natural Medicines

NUMB endocytic adaptor protein (NUMB) mediates the anti-hepatic fibrosis effect of artesunate (ART) by inducing senescence in hepatic stellate cells (HSCs)

Yangling Qiu, Yujia Li, Mengran Li, Yingqian Wang, Min Shen, Jiangjuan Shao, Feng Zhang, Xuefen Xu, Feixia Wang, Zili Zhang, Shizhong Zheng

Citation: Yangling Qiu, Yujia Li, Mengran Li, Yingqian Wang, Min Shen, Jiangjuan Shao, Feng Zhang, Xuefen Xu, Feixia Wang, Zili Zhang, Shizhong Zheng, NUMB endocytic adaptor protein (NUMB) mediates the anti-hepatic fibrosis effect of artesunate (ART) by inducing senescence in hepatic stellate cells (HSCs), Chinese Journal of Natural Medicines, 2025, 23(3), 322-333. doi: 10.1016/S1875-5364(25)60836-3.

View online: https://doi.org/10.1016/S1875-5364(25)60836-3

Wechat

Chinese Journal of Natural Medicines 23 (2025) 322-333

Contents lists available at ScienceDirect

Chinese Journal of Natural Medicines

journal homepage: www.cjnmcpu.com/

Original article

NUMB endocytic adaptor protein (NUMB) mediates the anti-hepatic fibrosis effect of artesunate (ART) by inducing senescence in hepatic stellate cells (HSCs)

Yangling Qiu[a], Yujia Li[a], Mengran Li[a], Yingqian Wang[a], Min Shen[b], Jiangjuan Shao[a], Feng Zhang[a], Xuefen Xu[a], Feixia Wang[a], Zili Zhang[a,*], Shizhong Zheng[a,*]

[a] *Jiangsu Key Laboratory for Pharmacology and Safety Evaluation of Chinese Materia Medica, Nanjing University of Chinese Medicine, Nanjing 210023, China*
[b] *Department of Biochemistry and Molecular Biology, Medical College, Yangzhou University, Yangzhou 225009, China*

ARTICLE INFO

Article history:
Received 21 December 2023
Revised 13 March 2024
Accepted 28 March 2024
Available online 20 March 2025

Keywords:
Hepatic stellate cells
NUMB endocytic adaptor protein
Senescence
Artesunate
Ubiquitylation
Liver fibrosis

ABSTRACT

Developing and identifying effective medications and targets for treating hepatic fibrosis is an urgent priority. Our previous research demonstrated the efficacy of artesunate (ART) in alleviating liver fibrosis by eliminating activated hepatic stellate cells (HSCs). However, the underlying mechanism remains unclear despite these findings. Notably, endocytic adaptor protein (NUMB) has significant implications for treating hepatic diseases, but current research primarily focuses on liver regeneration and hepatocellular carcinoma. The precise function of NUMB in liver fibrosis, particularly its ability to regulate HSCs, requires further investigation. This study aims to elucidate the role of NUMB in the anti-hepatic fibrosis action of ART in HSCs. We observed that the expression level of NUMB significantly decreased in activated HSCs compared to quiescent HSCs, exhibiting a negative correlation with the progression of liver fibrosis. Additionally, ART induced senescence in activated HSCs through the NUMB/P53 tumor suppressor (P53) axis. We identified NUMB as a crucial regulator of senescence in activated HSCs and as a mediator of ART in determining cell fate. This research examines the specific target of ART in eliminating activated HSCs, providing both theoretical and experimental evidence for the treatment of liver fibrosis.

1. Introduction

Liver fibrosis progression can culminate in cirrhosis and, in severe cases, lead to liver cancer development [1, 2]. Persistent liver fibrosis remains the primary cause of mortality among individuals with liver disease. Myofibroblasts, predominantly derived from activated hepatic stellate cells (HSCs), are the main contributors to extracellular matrix (ECM) secretion within the liver. Excessive ECM accumulation results in scarring and significant liver tissue damage, constituting the foremost pathological determinant of liver fibrosis [3]. Consequently, the elimination of activated HSCs emerges as a crucial focus in liver fibrosis treatment research. Inducing HSCs senescence stands as one of the effective antifibrotic strategies [4-6]. The principal manifestations of cellular senescence include sustained cell cycle arrest, DNA damage, telomerase shortening, and mitochondrial dysfunction [7]. Previous investigations by our research group have established that artesunate (ART), an artemisinin derivative extracted from Artemisia annua, exhibits antifibrotic properties and effectively eliminates activated HSCs [8]. Furthermore, ART has been documented to induce cellular senescence [9]. However, the precise regulatory influence of ART on HSCs senescence and the specific mechanisms require further elucidation.

The P53 tumor suppressor (P53) plays a central role in regulating cellular senescence. P53 responds to DNA damage, regulates P21 to inhibit cell cycle progression, and mediates mitochondrial damage and the senescence-associated secretory phenotype [10-12]. However, the specific role of P53 in ART-induced cellular senescence remains largely unexplored [13]. P53 has emerged as a crucial therapeutic target for various diseases [14]. Investigating the upstream regulators of P53 represents an effective approach to identifying key drivers of cellular senescence.

NUMB endocytic adaptor protein (NUMB), a cell-fate-determinant molecule, plays a regulatory role in various cellular activities, including autophagy, asymmetric division, and endocytosis [15-17]. A correlation has been identified between NUMB and cellular senescence, although the specific mechanism remains unclear [18]. Isabelle Le Roux *et al.* demonstrated that NUMB deficiency results in muscle cellular senescence [19]. However, it is well established that NUMB inhibits ubiquitination-mediated P53 protein degradation by forming a triple complex with P53 and the E3 ubiquitin ligase MDM2 proto-oncogene (MDM2) [20, 21]. This presents an intriguing question regarding whether NUMB regulates cellular senescence through P53. Notably, in this study, decreased NUMB expression was observed in activated HSCs compared to quiescent HSCs. This observation raises questions about

* Corresponding author.
E-mail addresses: njucm_zzl@163.com (Z. Zhang); nytws@163.com (S. Zheng)

https://doi.org/10.1016/S1875-5364(25)60836-3

the role of NUMB in regulating the fate of HSCs.

This investigation elucidated the role of ART in regulating HSCs. Additionally, it unveiled the regulatory function of NUMB in cellular senescence, enhanced understanding of the cellular senescence signaling network, and identified NUMB-dependent HSCs cellular senescence as a potential target for liver fibrosis treatment.

2. Materials and Methods

2.1. Plasmid construction

NUMB siRNA1-3 and P53 siRNA1-3 were obtained from KeyGEN BioTECH (Nanjing, China). pcDNA3.1-P53 was acquired from WeiZhen Biosciences (Jinan, China). As described in our previous research [22], we synthesized VA-Lip-Control-vector and VA-Lip-Numb-shRNA.

2.2. Animal experiment scheme

The animal experiment protocol was reviewed and approved by the Institutional Animal Protection and Use Committee of Nanjing University of Chinese Medicine. ICR mice (18−22 g) were maintained under pathogen-free conditions. To induce liver fibrosis, a mixture of CCl_4 and olive oil (1∶9, *V*/*V*) was administered intraperitoneally at a dosage of 0.1 mL/20 g body weight. Thirty Institute of Cancer Research (ICR) mice were randomly assigned to five groups of six mice each: control, CCl_4 only, CCl_4 with VA-Lip-control-vector, CCl_4 with VA-Lip-control-vector and ART, and CCl_4 with VA-Lip-Numb-shRNA and ART. Over 5 to 8 weeks, ART (20 mg·kg^{-1}, CAS:88495-63-0, K913007, DiBo Shanghai, China) was dissolved in olive oil and administered daily *via* intraperitoneal injection. VA-Lip-control-vector and VA-Lip-Numb-shRNA were prepared and injected *via* the caudal vein. Upon completion of the experiment, blood samples were collected from the orbital sinus, and the entire liver was excised. A portion of the liver tissue was preserved in fixation solution for histological analysis, while the remainder was stored at −80 °C for western blotting (WB) detection.

2.3. Histological analysis

The liver tissues were fixed, subjected to gradient dehydration, embedded in paraffin, and sectioned. Subsequently, the sections underwent hematoxylin-eosin (H&E) staining, Masson's trichrome staining, and Sirius Red staining as required. The results were then examined under a microscope.

2.4. Isolation and identification of mouse primary HSCs

The liver underwent a complete perfusion process, initially using a D-Hanks solution devoid of calcium and magnesium ions, administered through the hepatic portal vein. Subsequently, the liver was sequentially perfused with Streptomyces protease and type IV collagenase at appropriate concentrations. HSCs were then purified using Percoll discontinuous density gradient centrifugation. The viability of HSCs was assessed using the Trypan Blue exclusion method. Finally, the isolated HSCs were characterized through Desmin immunocytochemistry.

2.5. Cell culture

Immortalized and activated human HSCs LX2 (CL-0560) were obtained from Pricella (Wuhan, China). The cells were cultured in DMEM supplemented with 10% fetal bovine serum (FBS) and 1% antibiotics in an incubator maintained at 37 °C with 5% CO_2.

2.6. Transfection

The transfection process utilized a specific reagent (BMU111-CN, Abbkine, Wuhan, China) and followed the manufacturer's protocol. In brief, two separate mixtures were prepared: DNA-Opti-MEM and transfection agent-Opti-MEM. The latter was then gradually introduced into the DNA-Opti-MEM solution, gently homogenized using a pipette, and left to incubate at room temperature for 10−15 min prior to the transfection procedure.

2.7. MTT assay

Following 24-hour drug treatment, the culture medium in the 96-well plate was replaced with a fresh medium. A stock solution of 3-(4,5-dimethylthiazol-2-yl)-2,5-diphenyl-2*H*-tetrazolium bromide (MTT) at a concentration of 5 mg·mL^{-1} was prepared, and 20 μL of this solution was added to each well. After 4 h of incubation, the medium was removed, and 200 μL of dimethyl sulfoxide (DMSO) was added under light-protected conditions. Once the formazan crystals were fully dissolved, the absorbance at 490 nm was measured using a Multi-Detection Microplate Reader (Bio-Rad, Hercules, CA, USA).

2.8. WB assay

Cell or animal tissue was extracted using radioimmunoprecipitation assay (RIPA) lysate (P0013C, Beyotime, Shanghai, China). Protein concentration was measured using a microspectrophotometer (Nanodrop one, Thermo Fisher, USA). Sodium dodecyl sulfate (SDS) protein lysate (1×) was prepared and denatured at 95 °C for 15 min to obtain the sample. Proteins were transferred to a polyvinylidene fluoride (PVDF) membrane after gel electrophoresis and blocked with 5% skim milk powder for 2 h at room temperature. After incubation with the corresponding primary antibody at 4 °C for 16 h, the membrane was washed and incubated with the secondary antibody for 2 h. The antibodies used in this study are as follows: Albumin 16475-1-AP, Cytokeratin 19 14965-1-AP, F4/80 28463-1-AP, and α-smooth muscle actin (α-SMA) 14395-1-AP were obtained from Proteintech (Wuhan, China). CD31 AF6191 was purchased from Affinity (Nanjing, China). Collagen I ab138492, fibronectin ab268020, CDKN2A/ $p16^{INK4a}$ ab108349， and CDKN1A/$p21^{CIP1}$ ab109199 were acquired from Abcam (Cambridge, UK). P53 A3185, NUMB A9352, Cyclin A1/A2 A2635, Cyclin B1 A19037, β-actin AC026, and HRP-conjugated AffiniPure Mouse Anti-Rabbit IgG Light Chain AS061 were obtained from ABclonal (Wuhan, China). P53 2524T was purchased from CST (Shanghai, China). Puromycin MABE341 was acquired from Sigma-Aldrich (Burlington, USA). Images were developed by chemiluminescence and quantified using ImageJ.

2.9. RNA extract and real-time polymerase chain reaction (PCR)

Following the manufacturer's instructions, total RNA was extracted from LX2 cells using TRIzol (15596018, Invitrogen, USA). Subsequently, the extracted RNA was reverse transcribed to cDNA using a synthesis kit (RK20429, ABclonal, Wuhan, China). Real-time PCR was conducted using a quantitative SYBR Green PCR kit (RK21206, ABclonal, Wuhan, China) as per the provided protocol. The primers for *FN1*, *ACTA2*, *COL1A1*, *CDKN2A*, *CDKN1A*, *TP53*, *NUMB*, and *GAPDH* utilized in this study are detailed in Supplementary Table 1. The expression levels of target genes were normalized to GAPDH expression.

2.10. Wound healing assay

LX2 cells were seeded onto a 6-well plate at an appropriate

density. Once the cells adhered to form a monolayer, a p20 pipette tip was used to create equidistant scratches across the surface. Images were captured using a standard optical microscope immediately after scratching, designated as the 0 h time point. Subsequently, the medium was replaced with one containing mitomycin, and the cells were treated with the drug for 24 h. Following treatment, images were taken again, with three distinct regions photographed for each plate.

2.11. Morphological observation

The cells were seeded onto a 6-well plate and exposed to the drug for 24 h following adhesion. Cell morphology was subsequently documented using an optical microscope.

2.12. SA-β-Gal activity assay

The β-galactosidase staining kit was acquired from Xavier Biological Servicebio (G1073, Wuhan, China). Cells were fixed using the β-galactosidase stain fixing solution, prepared as per the manufacturer's instructions, and incubated with the cells at 37 °C for 36 h. Observation and image capture were performed using a standard light microscope.

2.13. Click-TM EdU incorporation assay

The kit was obtained from Beyotime (C0071, Shanghai, China) and utilized according to the manufacturer's instructions. Briefly, following a 2-hour incubation with EdU, the culture medium was removed, and the cells were fixed with 4% paraformaldehyde (PFA) for 15 min. Subsequently, the cells were washed and permeabilized with 0.3% Triton X-100 for 10 min. The Click reaction solution was then prepared and allowed to react with the cells for 30 min. Azide 488, with a maximum excitation wavelength of 495 nm and a maximum emission wavelength of 519 nm, was employed. The signal was detected using fluorescent enzyme labeling.

2.14. Analysis of cell-cycle disruptions

The cell cycle detection kit was obtained from KeyGEN BioTECH (KGA512, Nanjing, China) and utilized according to the manufacturer's instructions. Briefly, cells were harvested and fixed with 70% cold ethanol at 4 °C, then pre-treated with RNase A solution. Subsequently, propidium iodide (PI) dye was applied to label the cells. The excitation wavelength was set at 488 nm. Flow cytometry was employed to measure the results. Analysis of cell cycle distribution was conducted using Kaluza Analysis Software.

2.15. Immunohistofluorescence

For immunohistofluorescence analysis, PFA-fixed cells or cryosections underwent permeabilization with 0.2% Triton X-100, followed by incubation in a blocking buffer containing 3% bovine serum albumin (BSA) for 20 min. Subsequently, the sections were incubated with the specified primary antibodies overnight at 4 °C, followed by incubation with a secondary antibody for 1 h at room temperature. The sections were then stained with 4',6-diamidino-2-phenylindole (DAPI) (KGA215, KeyGEN, Nanjing, China) and examined using a confocal laser scanning microscope (Leica, Wetzlar, Germany).

2.16. Molecular docking

In accordance with the previously described methodology [23], the binding interaction between ART and NUMB (PDB: 5NJJ) was simulated utilizing AutoDock software.

2.17. Co-immunoprecipitation

The experiment was conducted according to established protocols. Briefly, a protein lysate containing 400–500 μg of protein was prepared. To this lysate, 3 μg of the target antibody was added and incubated for 2 h. Subsequently, blocked beads were introduced to the aforementioned protein lysate. Following a 2 h incubation on a shaker in an ice bath, magnetic bead separation, and denaturation elution were employed for WB analysis.

2.18. Cellular thermal shift assay (CETSA)

The specific experimental procedures can be found in liteurature [6] . In summary, following protein extraction, the cell lysate was divided into ten aliquots, which were then heated at temperatures of 43, 46, 49, 52, 55, 58, 61, 64, 67, and 79 degrees Celsius for three min each. Subsequently, these samples were prepared as 1× SDS protein lysates and analyzed using WB.

2.19. Gene Expression Omnibus (GEO) data analysis

GEO database (GSE25097) (https://www.ncbi.nlm.nih.gov/geo/geo2r/?acc=GSE25097) [24] and GEO database (GSE229155) (https://www.ncbi.nlm.nih.gov/geo/geo2r/?acc=GSE229155) [25] were utilized to analyze the NUMB expression level using GEO2R.

2.20. Statistical analysis

Data in this study were expressed as mean ± standard error of the mean (SEM). Statistical comparisons between two groups or multiple groups were conducted using Student's *t*-test or one-way analysis of variance followed by the Student-Newman-Keuls test, respectively. Prism 8.0 (GraphPad Software Inc, San Diego, CA) was employed to analyze the differences between groups. Statistical significance was established at $P < 0.05$.

3. Result

3.1. ART induces the senescence of activated HSCs in vitro

In vitro experiments utilized activated human HSCs (LX2) to investigate the specific mechanism of ART in counteracting liver fibrosis. ART demonstrated a dose-dependent inhibition of LX2 cell viability, with a notable effect evident starting at 10 μmol·L^{-1} (Fig. 1A). In subsequent experiments, LX2 cells were subjected to ART treatment at concentrations of 0, 5, 10, and 20 μmol·L^{-1}. The study first evaluated LX2 activation-related metrics. Results indicated that following ART treatment, both mRNA and protein expression levels of fibrosis markers, including *ACTA2*/α-SMA, *FN1*/fibronectin, and *COL1A1*/collagen I, were significantly reduced (Figs. 1B and 1C). Additionally, ART significantly inhibited the migratory capacity of LX2 cells (Fig. 1D). These findings suggest a dose-dependent inhibition of LX2 activation by ART.

Cytomorphological observations revealed that untreated cells predominantly exhibited fusiform or triangular shapes with markedly elongated tentacles, characteristic of activated LX2 cells (Fig. 2A) [26]. In contrast, ART-treated cells displayed an enlarged, flattened morphology, adopting irregular or polygonal shapes (Fig. 2A), consistent with cellular senescence characteristics [27-29]. To substantiate the hypothesis of ART-induced senescence in HSCs, further evaluation of relevant markers was conducted. A significant increase in SA-β-Gal staining-positive cells was observed in ART-treated cells compared to the control (Fig. 2B). Additionally, ART-treated LX2 cells entered a quiescent state, as indicated by negative EdU incorporation (Fig. 2C). The expression

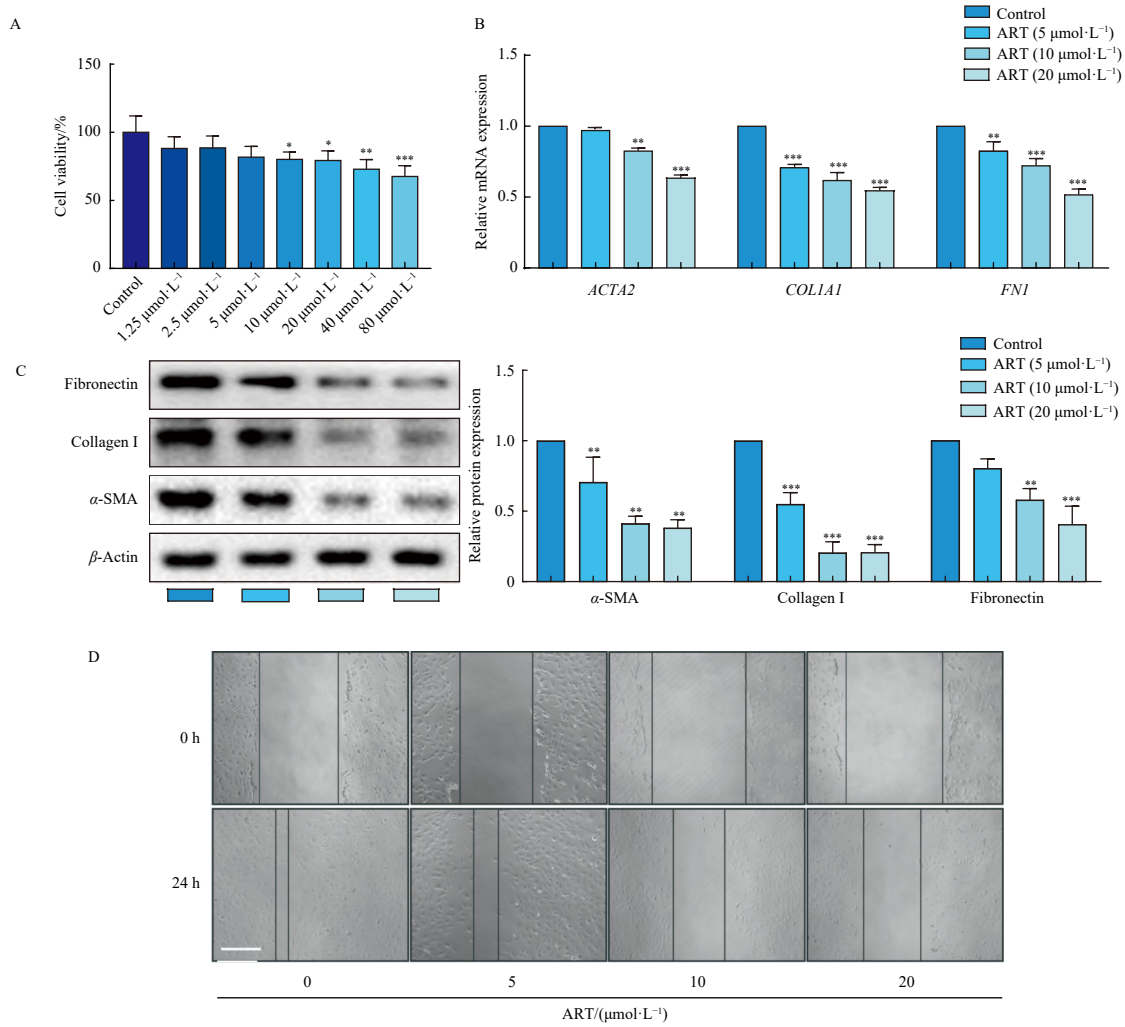

Fig. 1 ART dose-dependently inhibits the activation of HSCs *in vitro*. (A) LX2 cells were treated with 1.25, 2.5, 5, 10, 20, 40 and 80 μmol·L^{-1} ART for 24 h, respectively. Cell viability was assessed using the MTT assay, n = 6. (B) LX2 cells were exposed to 5, 10, and 20 μmol·L^{-1} ART for 24 h, respectively. mRNA levels were quantified *via* Real-Time PCR, n = 4. (C) Protein levels were determined through WB analysis, n = 3. (D) The migratory capacity of LX2 cells was evaluated using the Wound healing assay.Scale bar: 50 μm. Representative images were captured using ordinary light microscopes. $^{*}P < 0.05$, $^{**}P < 0.01$, $^{***}P < 0.001$ *vs* Con.

levels of key senescence markers, *CDKN2A*/p16^{INK4a} and *CDKN1A*/p21^{CIP1}, were also examined. Experimental results demonstrated a dose-dependent increase in both mRNA and protein expressions of *CDKN2A*/p16^{INK4a} and *CDKN1*A/p21^{CIP1} following ART treatment (Figs. 2D and 2E). Furthermore, the impact of ART on LX2 cell cycle progression was analyzed. Proper progression through the cell division cycle depends on the expression levels of corresponding cyclin proteins [30]. ART was found to dose-dependently suppress the expression of Cyclin A and Cyclin B (Fig. 2F), with Cyclin A involved in S phase DNA replication and Cyclin B playing a critical role in the transition from S to G_2 phase [30]. Cell cycle distribution, assessed using flow cytometry, consistently showed that ART arrested LX2 cells in the S phase (Fig. 2G). In conclusion, this study demonstrates that ART induces cellular senescence in activated HSCs.

3.2. ART regulates the senescence of activated HSCs via P53

The regulation of cellular senescence is significantly influenced by P53. In LX2 cells, ART treatment led to an increase in the protein level of P53 (Fig. 3A). Subsequently, we investigated whether ART regulates cellular senescence through the P53 pathway. The P53 plasmid was constructed and markedly increased the expression of P53 protein (Fig. 3B). P53 siRNA-1 was found to be the most effective in inhibiting P53 protein expression (Fig. 3C). Therefore, P53siRNA-1 and P53 plasmid were utilized in subsequent experiments. Interfering with P53 expression resulted in restored proliferative capacity and a reduction in the percentage of SA-β-Gal staining positive cells in ART-treated LX2 (Figs. 3D and 3E). The expression of senescence indicators P16 and P21 was attenuated (Fig. 3F), and cell cycle S phase checkpoint protein expression levels were recovered by P53 siRNA-1 (Fig. 3G). Additionally, the inhibition of cell migration and the expression of LX2 activation markers by ART were reversed upon interference with P53 (Figs. 3H and 3I). Conversely, the overexpression of P53 exacerbated the degree of senescence and inhibition in LX2 cells. These findings suggest that ART induces P53-dependent senescence in activated HSCs.

3.3. NUMB is required for ART-induced senescence of activated HSCs

NUMB, a cell fate regulator, is implicated in the progression of various diseases. However, its role in liver fibrosis remains unclear [31-33]. Analysis of the GSE25097 revealed reduced *NUMB* gene expression in liver fibrosis compared to normal tissue (Fig. 4A). Further examination of the GSE229155 demonstrated decreased *Numb* mRNA levels in TGF-β-stimulated HSCs relative to primary HSCs (Fig. 4B). To verify cell-specific alterations in NUMB expression during liver fibrosis, a mouse model was established using CCl_4. Primary HSCs were extracted from mice, with α-SMA serving as a key marker for HSCs activation [34]. Assessment of NUMB and α-SMA protein expression in primary mouse HSCs re-

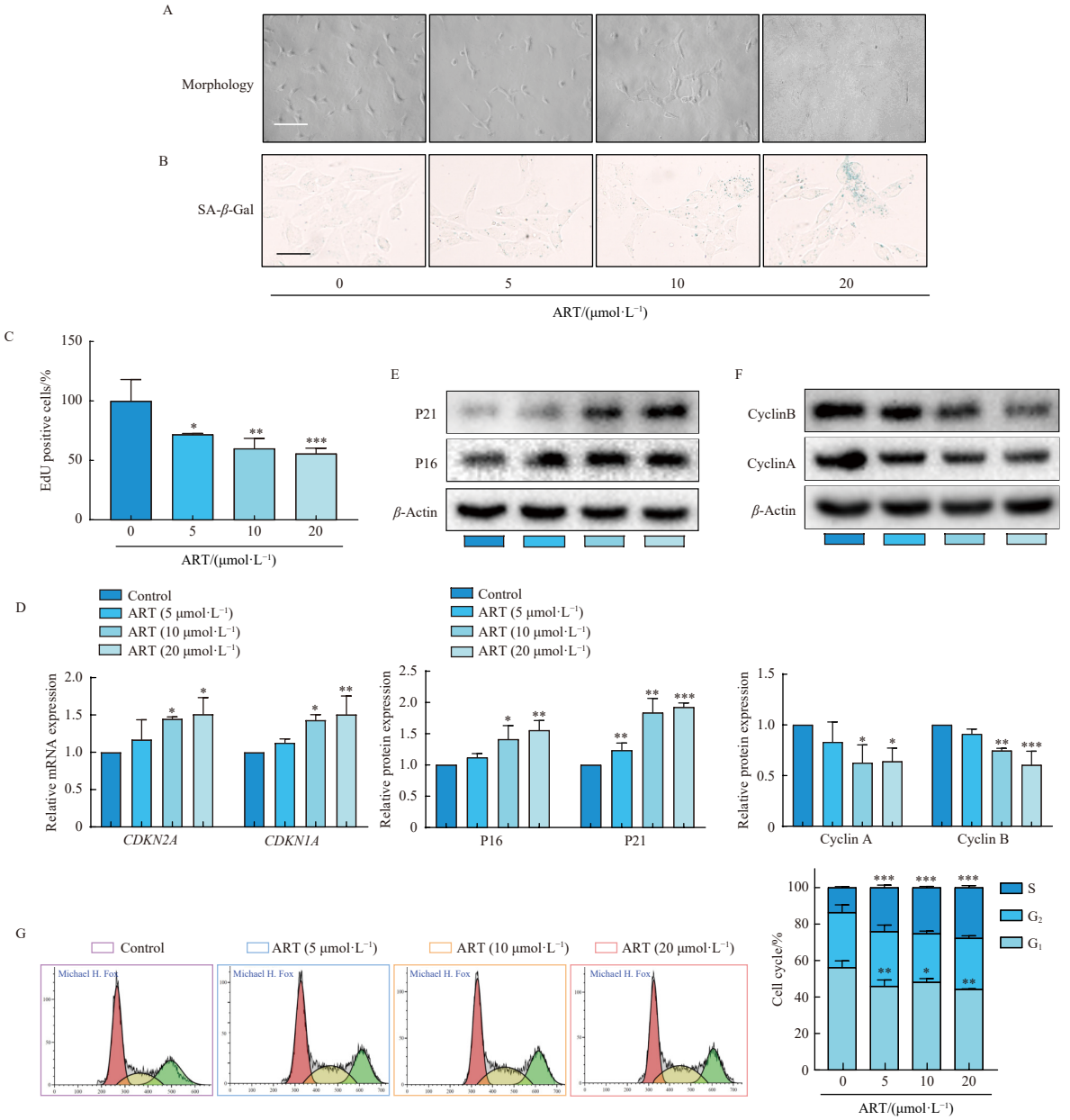

Fig. 2 ART induces HSCs senescence. LX2 cells were treated with 5, 10, and 20 μmol·L^{-1} ART for 24 h, respectively. (A) Representative images of cell morphology observed through standard light microscopy. Scale bar: 25 μm. (B) Representative images of SA-β-Gal staining of LX2 cells. Scale bar: 12.5 μm. (C) Quantification of EdU signal in cells, $n = 6$. (D) Real-time PCR assay detected the mRNA levels, $n = 4$. (E–F) The protein levels were detected by WB assay, $n = 3$. (G) Detection and quantification of LX2 cells cycle distribution, $n = 3$. $^{*}P < 0.05$, $^{**}P < 0.01$, $^{***}P < 0.001$ *vs* Con.

vealed down-regulation of NUMB protein in highly activated cells (Fig. 4C). Concurrently, tissue immunofluorescence staining was performed. Specific markers of major liver cell types, including α-SMA (for activated HSCs), Alb (Albumin, for hepatocytes), CD31 (for liver sinusoidal endothelial cells), CK19 (cytokeratin 19, for bile duct epithelium), and F4/80 (for Kupffer cells), were used to co-stain mouse liver tissue slices with NUMB. The results indicated that the distribution of the NUMB fluorescence signal closely corresponded to α-SMA positive cells. Moreover, the NUMB expression signal was significantly weakened in the co-localized regions of the liver fibrosis model (Fig. 4D). These findings suggest a negative correlation between NUMB expression in activated HSCs and liver fibrosis progression, indicating NUMB's potential role in modulating HSCs activation and fibrosis development.

Limited research has been conducted on NUMB's role in cellular senescence, despite its close association with P53. The potential involvement of NUMB in regulating P53-dependent cellular senescence through ART remains unclear. To investigate this, *NUMB* mRNA and protein levels were evaluated in ART-treated LX2 cells. The results demonstrated that ART promoted the accumulation of NUMB protein in a dose-dependent manner in activated LX2 cells, without affecting mRNA levels (Fig. 4E and 4F). This observation suggests that ART may regulate NUMB protein stability. Previous research indicates that ART can traverse the cell membrane and interact with proteins, potentially influencing their function [35]. Molecular docking analysis revealed a potential binding affinity between ART and NUMB (Fig. 4G). Specifically, the Ser155 amino acid residue of human NUMB (hNUMB) could form a crucial hydrogen bond with ART. The direct interaction between ART and NUMB was further confirmed through a temperature-dependent CETSA (Fig. 4H).

To investigate whether ART regulates the fate of activated HSCs *via* NUMB, we constructed NUMB siRNA, with siRNA-1 selected for subsequent experiments (Fig. 5A). NUMB siRNA-1 restored the proliferative capacity of LX2 cells treated with ART

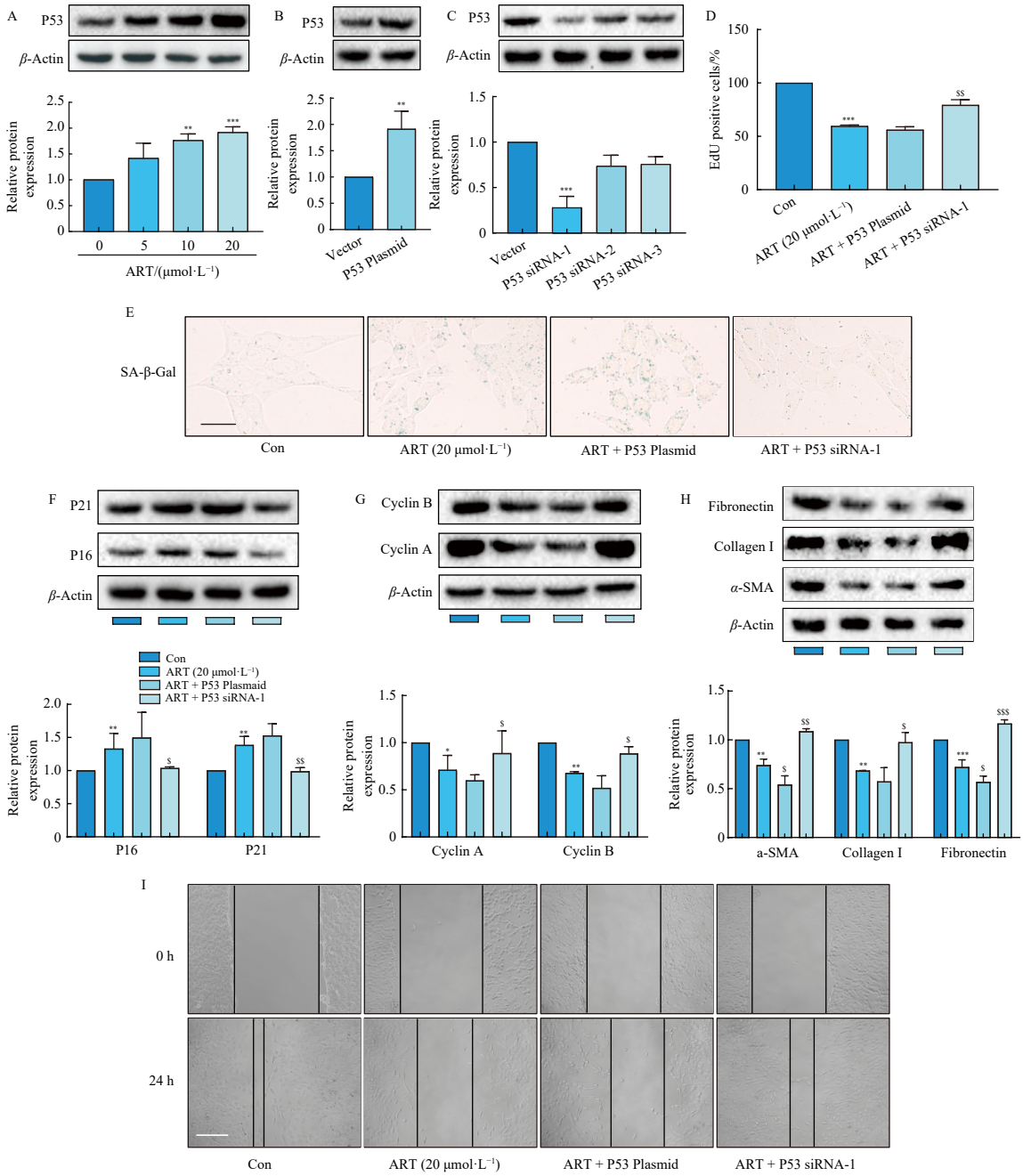

Fig. 3 ART induces P53-dependent HSCs senescence. (A–C) Protein levels were assessed using WB assay, $n = 3$. (D) LX2 cells were pre-transfected with vector, P53 plasmid, or P53 siRNA-1, followed by ART (20 μmol·L $^{-1}$) treatment for 24 h. EdU signal in cells was quantitatively detected, $n = 6$. (E) Representative image of SA-β-Gal staining in LX2 cells. Scale bar: 12.5 μm. (F–H) Protein levels were determined by WB assay, $n = 3$. (I) LX2 cells migration ability was evaluated using a wound healing assay. Scale bar: 50 μm.Typical images were captured using ordinary light microscopes. $^{*}P < 0.05$, $^{**}P < 0.01$, $^{***}P < 0.001$ *vs* Con; $^{\$}P < 0.05$, $^{\$\$}P < 0.01$, $^{\$\$\$}P < 0.001$ *vs* ART group.

(Fig. 5B). Interfering with NUMB expression reduced the number of SA-*β*-Gal staining-positive cells during ART treatment (Fig. 5C), inhibited the expression of ART-induced senescence markers (Fig. 5D), and reversed the ART-induced cell cycle arrest in LX2 cells (Figs. 5E and 5F). Additionally, the inhibitory effect of ART on the expression of *α*-SMA, collagen I, and fibronectin was significantly attenuated by NUMB interference (Fig. 5G). These findings suggest that ART modulates the activation and cellular senescence of activated HSCs through NUMB.

3.4. P53 is essential for NUMB to regulate the senescence of activated HSCs in ART treatment.

Research has demonstrated that NUMB regulates the ubiquitin-mediated degradation of the P53 protein [20]. We investigated whether NUMB influences ART's effect on P53. NUMB knockdown counteracted ART's regulation of P53 protein but not mRNA (Figs. 6A–6B), suggesting that NUMB regulated P53 at the protein level. Notably, ART administration significantly enhanced the binding of NUMB to P53 (Fig. 6C). Moreover, ART decelerated the degradation rate of the P53 protein, an effect nullified by NUMB interference (Fig. 6D). P53 is primarily degraded *via* the ubiquitination pathway [36]. Co-immunoprecipitation experiments revealed a reduction in P53 ubiquitination following ART treatment, an effect reversed upon NUMB knockdown (Fig. 6E). This demonstrates that ART's regulation of P53 protein stability is mediated by NUMB. A rescue experiment was conducted by introducing a P53 plasmid after NUMB interference. The results indicated that P53 replenishment restored LX2 cells' senescence markers (Figs. 6F–6H) and inhibited LX2 cells' activation indicat-

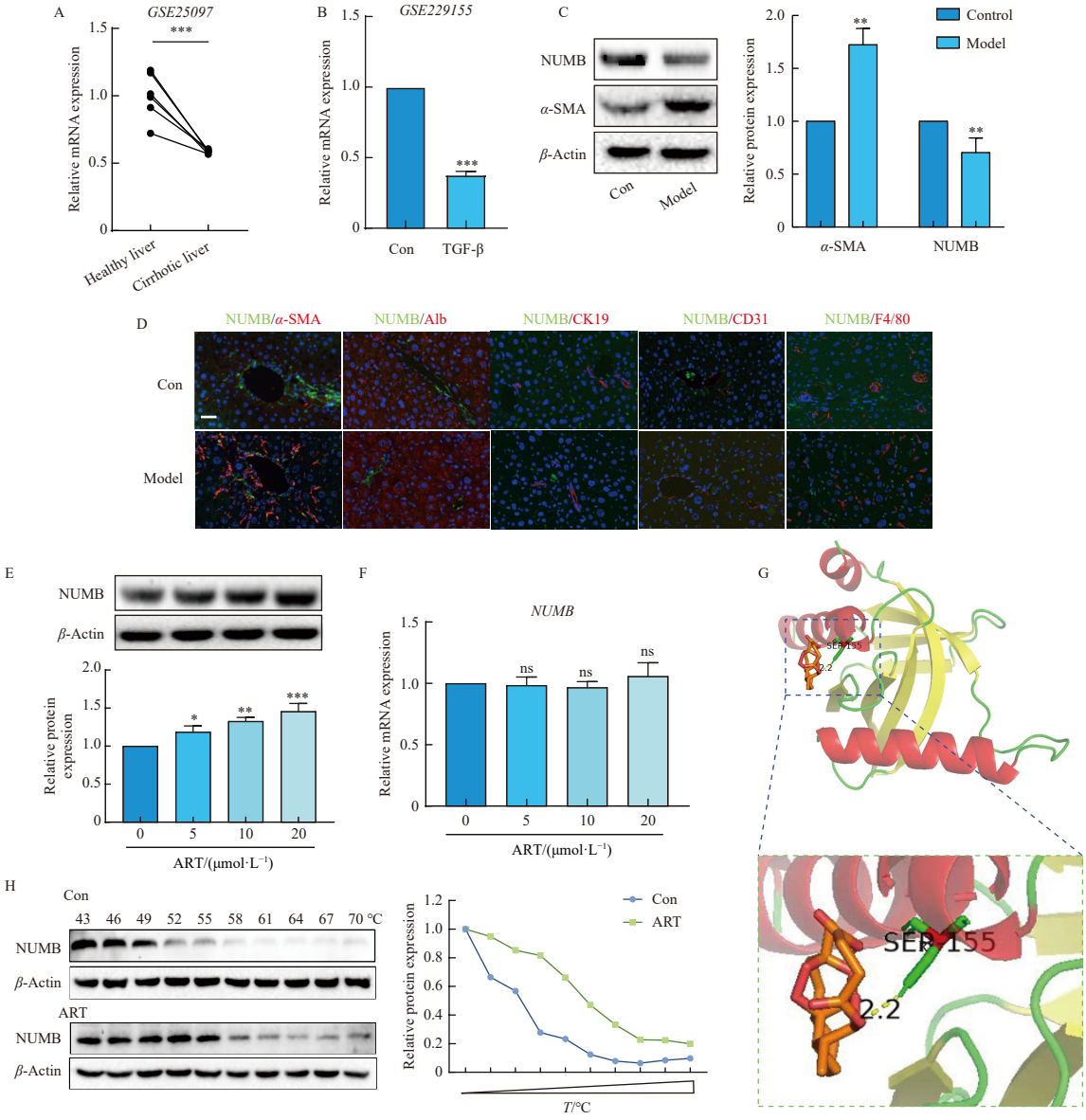

Fig. 4 NUMB is the target of ART in HSCs. (A) The expression level of *NUMB* mRNA in normal liver and cirrhotic tissues in the *GSE25097* cohort. $n = 6$. $^{*}P < 0.05$, $^{**}P < 0.01$, $^{***}P < 0.001$ *vs* Healthy liver group. (B) *NUMB* mRNA expression levels in the primary HSCs and TGF-β treated mouse HSCs in the *GSE229155* cohort, $n = 3$. $^{*}P < 0.05$, $^{**}P < 0.01$, $^{***}P < 0.001$ *vs* Con. (C) WB analysis revealed the content levels of NUMB and α-SMA protein, $n = 6$. $^{*}P < 0.05$, $^{**}P < 0.01$, $^{***}P < 0.001$ *vs* Con. (D) Immunofluorescence images of mouse healthy liver and fibrotic liver histologic sections. Scale bar: 25 μm. NUMB (green) co-stained with α-SMA (red), Albumin (red), CD31 (red), CK19 (red), and F4/80 (red). Nuclear staining with DAPI (blue). (E) WB were utilized to detect NUMB expression, $n = 3$. (F) Real-time PCR were utilized to detect NUMB expression, $n = 4$. $^{*}P < 0.05$, $^{**}P < 0.01$, $^{***}P < 0.001$ *vs* Con. (G) Expanded view of residues proximal to ART within the binding site. The highest-scoring pose is depicted. (H) WB assay was employed to detect NUMB protein, $n = 3$.

ors (Fig. 6I) in the context of combined ART and NUMB siRNA-1 treatment. These findings suggest that ART regulates the senescence of activated HSCs through the NUMB/P53 axis.

3.5. Targeted inhibition of NUMB in HSCs attenuates ART-mediated anti-hepatic fibrosis in mice.

In vitro, we have demonstrated a significant role of NUMB in the senescence of ART-induced activated HSCs. Subsequently, we investigated the role of NUMB in ART-mediated anti-hepatic fibrosis effects *in vivo*. Compared to the normal group, the liver surface in the model group exhibited roughness and fibrotic lesions. ART treatment alleviated CCl_4-induced liver fibrosis (Fig. 7A). However, pretreatment with VA-Lip-Numb-shRNA diminished the ameliorative effect of ART on liver fibrosis in mice (Fig. 7A). Additionally, pretreatment with *Numb* gene knockdown in HSCs intensified vacuolation, necrosis, and collagen deposition in the liver tissue, compared to the group treated only with ART (Fig. 7A). For a more comprehensive assessment of hepatic fibrosis in mice, we examined the accumulation of α-SMA and fibronectin in mouse liver tissues. The results corroborated the above findings (Fig. 7B). These observations suggest that NUMB in HSCs mediates the anti-hepatic fibrosis effect of ART.

To further validate the regulation of ART in HSC senescence through NUMB *in vivo*, we conducted co-staining of α-SMA with NUMB and P53 separately. Compared to the model group, α-SMA expression was significantly reduced following ART treatment, while the signals of NUMB and P53 in regions co-localizing with α-SMA were individually enhanced. However, this effect was reversed upon *Numb* knockdown in HSCs (Figs. 8A and 8B). Primary HSCs were extracted from mouse livers for protein detection. Consistently, it was also demonstrated that the expression of NUMB and P53 was inversely correlated with the activation state of primary HSCs at the protein level (Fig. 8C). These

findings support that NUMB mediates the impact of ART on P53 in HSCs. Concurrently, we evaluated the expression of senescence-related indicators in primary HSCs. The levels of P16 and P21 significantly increased after ART administration, and this effect was reversed after *Numb* knockdown (Fig. 8D). The *in vivo* experimental assays further confirm that ART upregulates NUMB to induce senescence in activated HSCs, thereby exerting an anti-hepatic fibrosis effect.

4. Discussion

NUMB plays a crucial role in determining cell fate. During tumor progression, cancer cells often exhibit reduced NUMB expression, as demonstrated by previous studies [37-39]. Moreover, increased NUMB levels have been associated with cell death [33]. These findings suggest that targeting NUMB in HSCs could be an effective antifibrosis strategy. In a mouse model of liver fibrosis, NUMB showed an inverse correlation specifically with α-SMA expression, in the mouse model of liver fibrosis, indicating a negative relationship between NUMB and HSCs activation. The inhibitory role of NUMB in HSC activation was further confirmed through primary HSCs assays and *in vitro* NUMB interference experiments. Consequently, enhancing NUMB expression or activity may impede the critical functions of activated HSCs, potentially offering a pathway to combat liver fibrosis. However, additional studies are required to establish a definitive causal relationship between HSC activation and decreased NUMB expression.

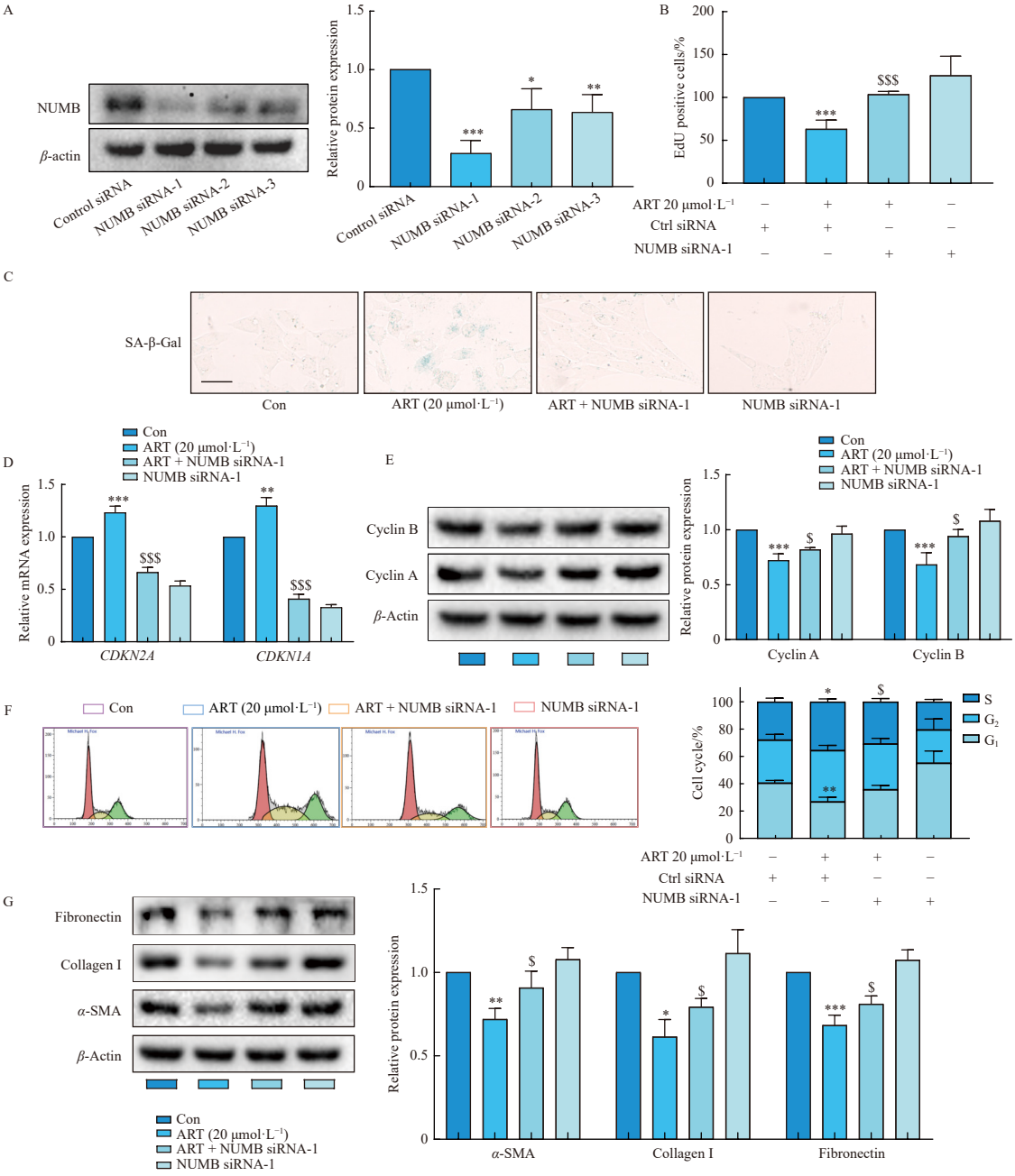

Fig. 5 NUMB is essential for ART-mediated regulation of senescence in HSCs. (A) WB analysis of NUMB protein expression, n = 3. (B) LX2 cells were pre-transfected with vector or NUMB siRNA-1, followed by treatment ART (20 μmol·L^{-1}) for 24 h or left untreated. Quantitative analysis of EdU signal to assess LX2 cell proliferation, n = 6. (C) Representative images of β-galactosidase activity in LX2 cells.Scale bar: 12.5 μm. (D) mRNA levels determined by Real-Time PCR, n = 4. (E) Protein levels and quantification assessed by WB assay, n = 3. (F) Analysis and quantification of LX2 cell cycle distribution, n = 3. (G) Protein levels detected by WB assay, n = 3. $^{*}P < 0.05$, $^{**}P < 0.01$, $^{***}P < 0.001$ *vs* Con; $^{\$}P < 0.05$, $^{\$\$}P < 0.01$, $^{\$\$\$}P < 0.001$ *vs* ART group.

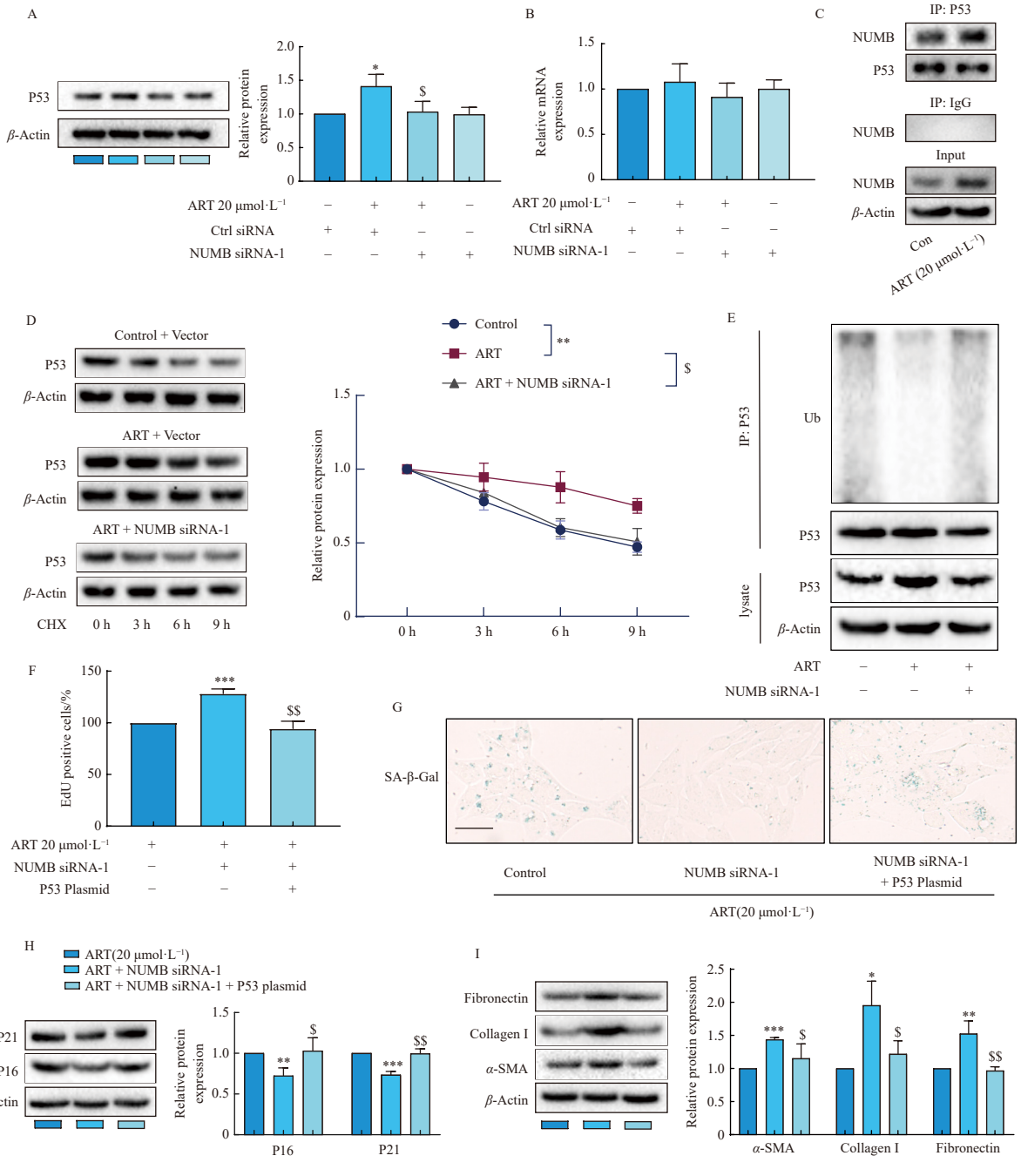

Fig. 6 ART regulates HSCs senescence *via* the NUMB/P53 axis. (A) WB were utilized to assess P53 expression, $n = 3$. $^{*}P < 0.05$, $^{**}P < 0.01$, $^{***}P < 0.001$ *vs* Con; $^{\$}P < 0.05$, $^{\$\$}P < 0.01$, $^{\$\$\$}P < 0.001$ *vs* ART group. (B) Real-Time PCR were utilized to assess P53 expression, $n = 4$. (C) An immunoprecipitation assay was conducted to examine the binding of P53 to NUMB. (D) LX2 cells, pre-transfected with vector or NUMB siRNA-1, were subsequently treated with ART (20 μmol·L^{-1}) and cycloheximide (CHX) for 3, 6, and 9 h. P53 protein was detected *via* WB. $n = 3$. $^{*}P < 0.05$, $^{**}P < 0.01$, $^{***}P < 0.001$ *vs* Con; $^{\$}P < 0.05$, $^{\$\$}P < 0.01$, $^{\$\$\$}P < 0.001$ *vs* ART group. (E) An immunoprecipitation assay was performed to analyze the binding of ubiquitin to P53. (F) Following transfection with NUMB siRNA-1 or P53 plasmid, LX2 cells were treated with ART (20 μmol·L^{-1}) for 24 h. $^{*}P < 0.05$, $^{**}P < 0.01$, $^{***}P < 0.001$ *vs* ART group; $^{\$}P < 0.05$, $^{\$\$}P < 0.01$, $^{\$\$\$}P < 0.001$ *vs* ART + NUMB siRNA-1 group. Quantitative detection of EdU signals was used to assess the proliferation capacity of LX2 cells, $n = 6$. (G) Representative image of SA-β-Gal staining of LX2 cells. Scale bar: 12.5 μm. (H–I) Protein levels were determined by WB assay. $n = 3$. $^{*}P < 0.05$, $^{**}P < 0.01$, $^{***}P < 0.001$ *vs* ART group; $^{\$}P < 0.05$, $^{\$\$}P < 0.01$, $^{\$\$\$}P < 0.001$ *vs* ART + NUMB siRNA-1 group.

ART has been documented to trigger cellular senescence in colorectal cancer cells and glioma cells [9, 13]. However, this effect has not been observed in HSCs, and there is limited research on ART-induced cellular senescence, with the specific regulatory mechanism remaining unclear. In this study, we initially confirmed that ART induces senescence in activated HSCs. P53 plays a crucial role in regulating cellular senescence. To further investigate the mechanism of ART, we employed P53 plasmid and siRNA to assess the impact of ART on P53-dependent senescence. It is established that the binding of NUMB to P53 regulates the stability of the P53 protein, with the theory of NUMB binding to P53 well-documented [21, 40]. We sought to determine whether ART regulates P53 proteins through NUMB. Through molecular docking and CETSA experiments, we discovered that ART binds to NUMB protein. Additionally, ART promotes the stabilization of NUMB protein, suggesting its potential as a NUMB agonist. Further *in vitro* and *in vivo* experiments revealed that knockdown of NUMB impaired ART-induced senescence in activated HSCs, implying that ART induces senescence through NUMB in HSCs. To verify that NUMB regulates cellular senescence through P53, we performed a P53 backfill experiment. In the absence of NUMB, the addition of a P53 overexpression plasmid rescued ART-in-

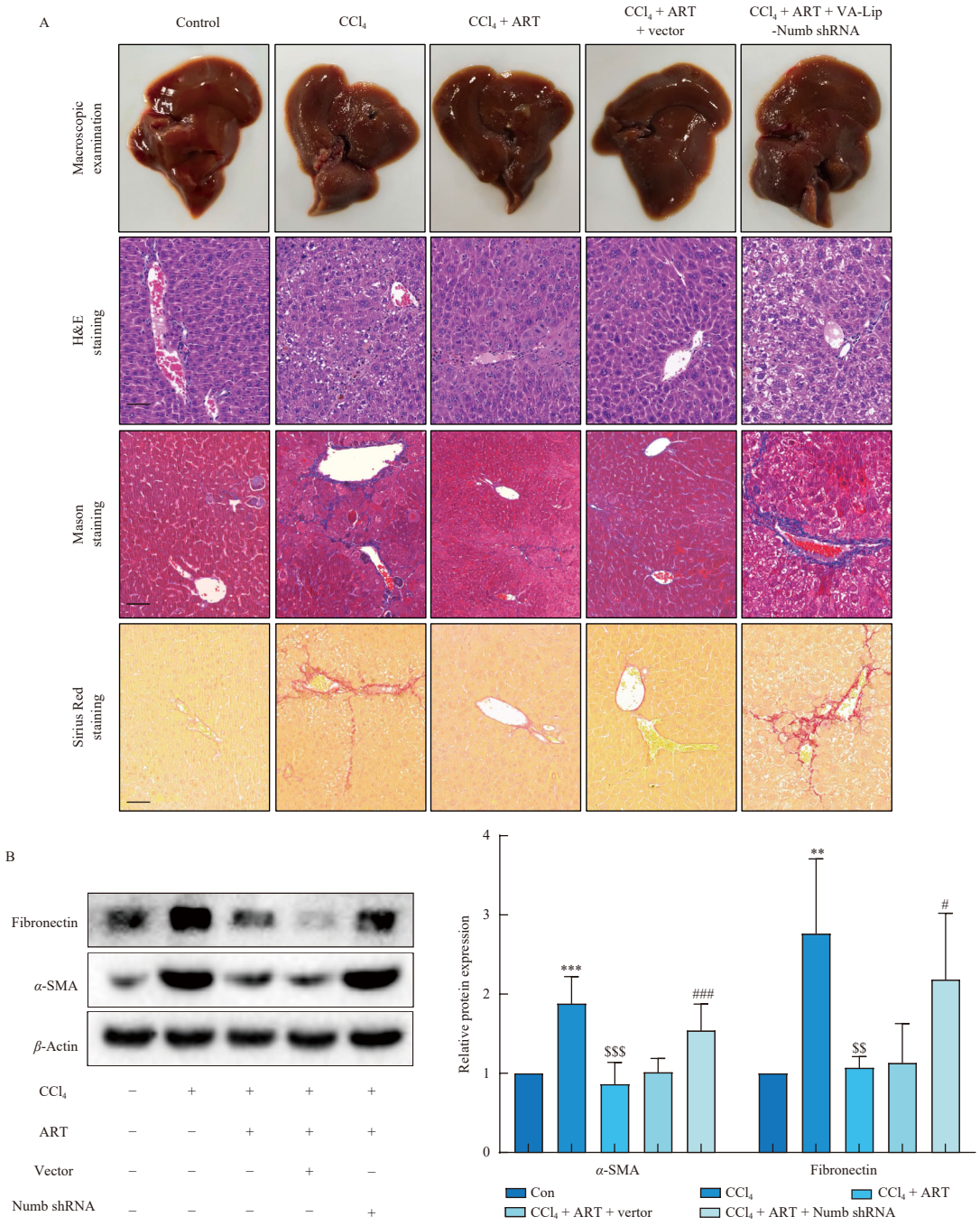

Fig. 7 Knockdown of *Numb* gene in HSCs attenuates the anti-hepatic fibrosis effect of ART *in vivo*. (A) Mouse livers were extracted, and representative images were captured, followed by pathological examinations. Scale bar: 50 μm. (B) WB analysis was conducted, $n = 5$. $^{*}P < 0.05$, $^{**}P < 0.01$, $^{***}P < 0.001$ *vs* Con; $^{\$}P < 0.05$, $^{\$\$}P < 0.01$, $^{\$\$\$}P < 0.001$ *vs* CCl_4 group; $^{\#}P < 0.05$, $^{\#\#}P < 0.01$, $^{\#\#\#}P < 0.001$ *vs* CCl_4 + ART group.

duced senescence in HSCs. These findings unveil a novel pathway for ART to regulate cellular senescence and partially elucidate the role of NUMB in this process.

The elimination of activated HSCs is a central focus in liver fibrosis treatment, with numerous studies and preclinical drug developments currently addressing this issue. Our research indicates that NUMB is inversely correlated with the activation state of HSCs. Importantly, we discovered that NUMB is a significant target for ART regulation of P53-mediated HSCs senescence, offering novel avenues for drug therapy strategies targeting HSCs and identifying potential therapeutic targets.

5. Conclusion

This study demonstrates that during liver fibrosis, NUMB expression is downregulated when HSCs are activated. The accumulation of NUMB induces HSC senescence by inhibiting P53 degradation under the influence of ART (Fig. S1). Our research elucidates the molecular mechanism of ART-induced senescence and identifies NUMB as a potential therapeutic target for liver fibrosis treatment.

Funding

The work was supported by the National Natural Science Foundation of China (Nos. 82474164, 82374124, 82073914, 82173874, 82274185, 82305046 and 82304902), the Natural Science Foundation of Jiangsu Province (Nos. BK20230458 and BK20220467), the General Project of the Natural Science Research of Jiangsu Higher Education Institutions (No.

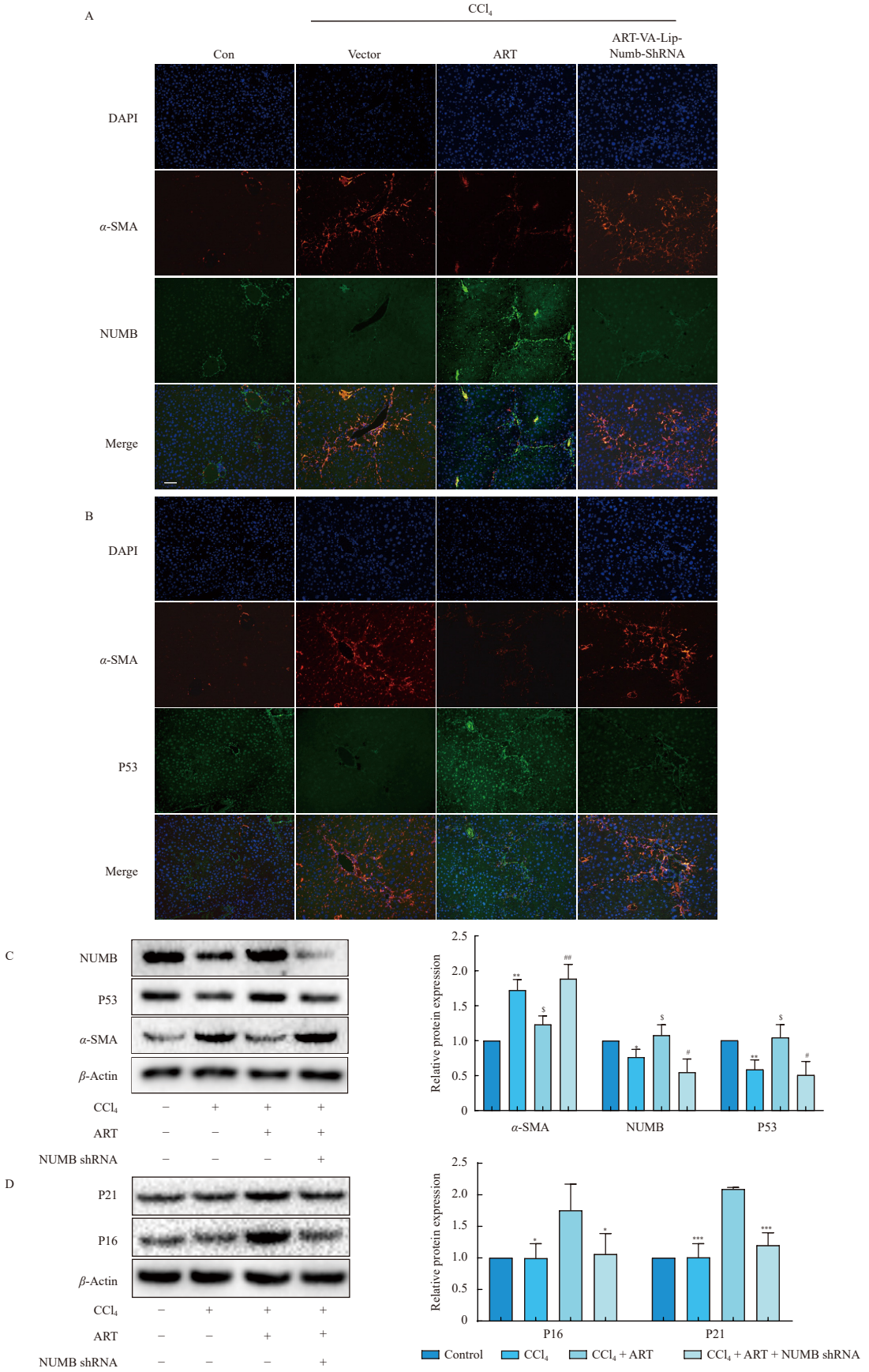

Fig. 8 NUMB mediates ART-induced HSCs senescence *in vivo*. (A–B) Representative images of α-SMA (red) co-stained with NUMB (green) and P53 (green) detected by immunofluorescence in mouse liver sections. Nuclei stained with DAPI (blue), Scale bar: 50μm. (C) Protein levels in primary HSCs isolated from mouse liver detected by WB, $n = 5$. $^{*}P < 0.05$, $^{**}P < 0.01$, $^{***}P < 0.001$ vs Con; $^{\$}P < 0.05$, $^{\$\$}P < 0.01$, $^{\$\$\$}P < 0.001$ *vs* CCl_4 group; $^{\#}P < 0.05$, $^{\#\#}P < 0.01$, $^{\#\#\#}P < 0.001$ *vs* CCl_4 + ART group. (D) Protein levels in primary HSCs isolated from mouse liver determined by WB, $n = 5$. $^{*}P < 0.05$, $^{**}P < 0.01$, $^{***}P < 0.001$ *vs* CCl_4 + ART group.

23KJB310017), and Young Elite Scientists Sponsorship Program by CACM (No. 2022-QNRC2-B15).

Supporting Information

Supporting information for this study is available upon request via email to the corresponding authors.

Declaration of competing interest

These authors have no conflict of interest to declare.

References

1 Li N, Zhang X, Zhou J, et al. Multiscale biomechanics and mechanotransduction from liver fibrosis to cancer. *Adv Drug Deliver Rev*. 2022;188:114448. https://doi.org/10.1016/j.addr.2022.114448.
2 Yang X, Li Q, Liu W, et al. Mesenchymal stromal cells in hepatic fibrosis/cirrhosis: from pathogenesis to treatment. *Cell Mol Immunol*. 2023;20(6):583-599. https://doi.org/10.1038/s41423-023-00983-5.
3 Tsuchida T, Friedman SL. Mechanisms of hepatic stellate cell activation. *Nat Rev Gastro Hepat*. 2017;14(7):397-411. https://doi.org/10.1038/nrgastro.2017.38.
4 Du K, Maeso-Diaz R, Oh SH, et al. Targeting YAP-mediated HSC death susceptibility and senescence for treatment of liver fibrosis. *Hepatology*. 2023;77(6):1998-2015. https://doi.org/10.1097/HEP.0000000000000326.
5 Higashi T, Friedman SL, Hoshida Y. Hepatic stellate cells as key target in liver fibrosis. *Adv Drug Deliver Rev*. 2017;121:27-42. https://doi.org/10.1016/j.addr.2017.05.007.
6 Wang F, Li Z, Chen L, et al. Inhibition of ASCT2 induces hepatic stellate cell senescence with modified proinflammatory secretome through an IL-1α/NF-kappaB feedback pathway to inhibit liver fibrosis. *Acta Pharm Sin B*. 2022;12(9):3618-3638. https://doi.org/10.1016/j.apsb.2022.03.014.
7 Miwa S, Kashyap S, Chini E, et al. Mitochondrial dysfunction in cell senescence and aging. *J Clin Invest*. 2022;132(13):e158447. https://doi.org/10.1172/JCI158447.
8 Wang Y, Li Y, Qiu Y, et al. Artesunate induces ferroptosis in hepatic stellate cells and alleviates liver fibrosis *via* the ROCK1/ATF3 axis. *J Clin Transl Hepato*. 2024;12(1):36-51. https://doi.org/10.14218/JCTH.2023.00162.
9 Huang Z, Gan S, Zhuang X, et al. Artesunate inhibits the cell growth in colorectal cancer by promoting ROS-dependent cell senescence and autophagy. *Cells*. 2022;11(16):2472. https://doi.org/10.3390/cells11162472.
10 Wu D, Prives C. Relevance of the p53-MDM2 axis to aging. *Cell Death Differ*. 2018;25(1):169-179. https://doi.org/10.1038/cdd.2017.187.
11 Aubrey BJ, Kelly GL, Janic A, et al. How does p53 induce apoptosis and how does this relate to p53-mediated tumour suppression? *Cell Death Differ*. 2018;25(1):104-113. https://doi.org/10.1038/cdd.2017.169.
12 Ou HL, Schumacher B. DNA damage responses and p53 in the aging process. *Blood*. 2018;131(5):488-495. https://doi.org/10.1182/blood-2017-07-746396.
13 Wei S, Liu L, Chen Z, et al. Artesunate inhibits the mevalonate pathway and promotes glioma cell senescence. *J Cell Mol Med*. 2020;24(1):276-284. https://doi.org/10.1111/jcmm.14717.
14 Wang H, Guo M, Wei H, et al. Targeting p53 pathways: mechanisms, structures, and advances in therapy. *Signal Transduct Tar*. 2023;8(1):92. https://doi.org/10.1038/s41392-023-01347-1.
15 Li H, Shu S, Zhou M, et al. NUMB facilitates autophagy initiation through targeting $SCF^{\beta\text{-}TrCP2}$ complex. *Cell Death Differ*. 2022;29(7):1409-1422. https://doi.org/10.1038/s41418-022-00930-3.
16 Belle VA, McDermott N, Meunier A, et al. NUMB inhibition of NOTCH signalling as a therapeutic target in prostate cancer. *Nat Rev Urol*. 2014;11(9):499-507. https://doi.org/10.1038/nrurol.2014.195.
17 Wu MJ, Chen YS, Kim MR, et al. Epithelial-mesenchymal transition directs stem cell polarity *via* regulation of mitofusin. *Cell Metab*. 2019;29(4):993-1002, e1006. https://doi.org/10.1016/j.cmet.2018.11.004.
18 Conboy IM, Conboy MJ, Smythe GM, et al. Notch-mediated restoration of regenerative potential to aged muscle. *Science*. 2003;302(5650):1575-1577. https://doi.org/10.1126/science.1087573.
19 Le Roux I, Konge J, Le Cam L, et al. Numb is required to prevent p53-dependent senescence following skeletal muscle injury. *Nat Commun*. 2015;6:8528. https://doi.org/10.1038/ncomms9528.
20 Carter S, Vousden KH. A role for Numb in p53 stabilization. *Genome Biol*. 2008;9(5):221. https://doi.org/10.1186/gb-2008-9-5-221.
21 Colaluca IN, Tosoni D, Nuciforo P, et al. NUMB controls p53 tumour suppressor activity. *Nature*. 2008;451(7174):76-80. https://doi.org/10.1038/nature06412.
22 Shen M, Li Y, Wang Y, et al. N^6-methyladenosine modification regulates ferroptosis through autophagy signaling pathway in hepatic stellate cells. *Redox Biol*. 2021;47:102151. https://doi.org/10.1016/j.redox.2021.102151.
23 Forli S, Huey R, Pique ME, et al. Computational protein-ligand docking and virtual drug screening with the AutoDock suite. *Nat Protoc*. 2016;11(5):905-919. https://doi.org/10.1038/nprot.2016.051.
24 Tung EK, Mak CK, Fatima S, et al. Clinicopathological and prognostic significance of serum and tissue Dickkopf-1 levels in human hepatocellular carcinoma. *Liver Int*. 2011;31(10):1494-1504. https://doi.org/10.1111/j.1478-3231.2011.02597.x.
25 Rho H, Terry AR, Chronis C, et al. Hexokinase 2-mediated gene expression *via* histone lactylation is required for hepatic stellate cell activation and liver fibrosis. *Cell Metab*. 2023;35(8):1406-1423, e1408. https://doi.org/10.1016/j.cmet.2023.06.013.
26 Sufletel RT, Melincovici CS, Gheban BA, et al. Hepatic stellate cells - from past till present: morphology, human markers, human cell lines, behavior in normal and liver pathology. *Rom J Morphol Embryol*. 2020;61(3):615-642. https://doi.org/10.47162/RJME.61.3.01.
27 Lanz MC, Zatulovskiy E, Swaffer MP, et al. Increasing cell size remodels the proteome and promotes senescence. *Mol Cell*. 202;82(17):3255-3269, e3258. https://doi.org/10.1016/j.molcel.2022.07.017.
28 Krizhanovsky V, Yon M, Dickins RA, et al. Senescence of activated stellate cells limits liver fibrosis. *Cell*. 2008;134(4):657-667. https://doi.org/10.1016/j.cell.2008.06.049.
29 Hernandez-Segura A, Nehme J, Demaria M. Hallmarks of cellular senescence. *Trends Cell Biol*. 2018;28(6):436-453. https://doi.org/10.1016/j.tcb.2018.02.001.
30 Martinez-Alonso D, Malumbres M. Mammalian cell cycle cyclins. *Semin Cell Dev Biol*. 2020;107:28-35. https://doi.org/10.1016/j.semcdb.2020.03.009.
31 Li MR, Lei CT, Tang H, et al. MAD2B promotes podocyte injury through regulating Numb-dependent Notch 1 pathway in diabetic nephropathy. *Int J Biol Sci*. 2022;18(5):1896-1911. https://doi.org/10.7150/ijbs.68977.
32 Hristova DM, Fukumoto T, Takemori C, et al. NUMB as a therapeutic target for melanoma. *J Invest Dermatol*. 2022;142(7):1882-1892,e1885. https://doi.org/10.1016/j.jid.2021.11.027.
33 Lacomme M, Hales SC, Brown TW, et al. Numb regulates Tau levels and prevents neurodegeneration in tauopathy mouse models. *Sci Adv*. 2022;8(42):eabm4295. https://doi.org/10.1126/sciadv.abm4295.
34 Schinagl M, Tomin T, Gindlhuber J, et al. Proteomic changes of activated hepatic stellate cells. *Int J Mol Sci*. 2021;22(23):12782. https://doi.org/10.3390/ijms222312782.
35 Hahn F, Niesar A, Wangen C, et al. Target verification of artesunate-related antiviral drugs: assessing the role of mitochondrial and regulatory proteins by click chemistry and fluorescence labeling. *Antivir Res*. 2020;180:104861. https://doi.org/10.1016/j.antiviral.2020.104861.
36 Yuan J, Luo K, Zhang L, et al. USP10 regulates p53 localization and stability by deubiquitinating p53. *Cell*. 2010;140(3):384-396. https://doi.org/10.1016/j.cell.2009.12.032.
37 Qin X, Cao Y. Prognostic biomarker NUMB is inhibited by breast cancer cell exosomes to promote breast cancer progression. *J Immunol Res*. 2022;2022:6032076. https://doi.org/10.1155/2022/6032076.
38 Shu Y, Xu Q, Xu Y, et al. Loss of Numb promotes hepatic progenitor expansion and intrahepatic cholangiocarcinoma by enhancing Notch signaling. *Cell Death Dis*. 2021;12(11):966. https://doi.org/10.1038/s41419-021-04263-w.
39 Ortega-Campos SM, Garcia-Heredia JM. The multitasker protein: a look at the multiple capabilities of NUMB. *Cells*. 2023;12(2):333. https://doi.org/10.3390/cells12020333.
40 Dhami GK, Liu H, Galka M, et al. Dynamic methylation of Numb by Set8 regulates its binding to p53 and apoptosis. *Mol Cell*. 2013;50(4):565-576. https://doi.org/10.1016/j.molcel.2013.04.028.